Université de Montréal

In Vivo Phosphorus Spectroscopy in Human Subjects on a Clinical 3T MRI system

by

Brice Tiret

Institut de Génie Biomédical, Université de Montréal

Mémoire présenté à la Faculté de Médecine
en vue de l'obtention du grade de Master
en Génie Biomédical
Option Imagerie et Instrumentation

Avril 2013

Résumé

Alors que l'Imagerie par résonance magnétique (IRM) permet d'obtenir un large éventail de données anatomiques et fonctionnelles, les scanneurs cliniques sont généralement restreints à l'utilisation du proton pour leurs images et leurs applications spectroscopiques. Le phosphore jouant un rôle prépondérant dans le métabolisme énergétique, l'utilisation de cet atome en spectroscopie RM présente un énorme avantage dans l'observation du corps humain. Cela représente un certain nombre de défis techniques à relever dus à la faible concentration de phosphore et sa fréquence de résonance différente. L'objectif de ce projet a été de développer la capacité à réaliser des expériences de spectroscopie phosphore sur un scanneur IRM clinique de 3 Tesla. Nous présentons ici les différentes étapes nécessaires à la conception et la validation d'une antenne IRM syntonisée à la fréquence du phosphore. Nous présentons aussi l'information relative à réalisation de fantômes utilisés dans les tests de validation et la calibration. Finalement, nous présentons les résultats préliminaires d'acquisitions spectroscopiques sur un muscle humain permettant d'identifier les différents métabolites phosphorylés à haute énergie. Ces résultats s'inscrivent dans un projet de plus grande envergure où les impacts des changements du métabolisme énergétique sont étudiés en relation avec l'âge et les pathologies.

Mots-clés : IRM, spectroscopie, phosphore, métabolisme, antenne

Abstract

Although magnetic resonance imaging (MRI) provides a wide array of anatomical and functional contrasts, clinical MRI systems are typically limited to imaging of tissue water and spectroscopy based on hydrogen atoms in more complex molecules. Given the important role of phosphate metabolism in virtually all biological processes, there has been considerable interest in the development of technology allowing detection and spectroscopy of magnetic resonance signals associated with phosphorus in the human body. This poses a number of technical challenges, due to the lower natural abundance and resonant frequency of phosphorus. The objective of this project was to develop and implement a basic in vivo phosphorus capability on a clinical 3 Tesla MRI scanner. We present here the various steps toward building and testing a working prototype of MR coil tuned to phosphorus frequency. We also provide information on building a set of test phantoms required for this project that can be used for signal calibration. Finally we show preliminary phosphorus spectra from muscle, in human subjects, demonstrating the main constituents in high-energy phosphate metabolism. These results pave the way for future applications in which the metabolic physiology of the human brain will be studied during aging and in disease.

Keywords : MRI, Spectroscopy, Phosphorus, Metabolism, Coil

Content Table

Figures List

Tables List

Abbreviations and acronyms

AD	Alzheimer's Disease
ATP	Adenosine Tri Phosphate
BOLD	Blood oxygen level-dependent
CBF	Cerebral blood flow
*fid	Free induction decay sequence
Lac	Lactate
MCI	Mild cognitive impairment
mM	milli-Molar
MRI	Magnetic Resonance Imaging
NAA	N-Acetyl-Aspartate
PCr	Phosphocreatine
PD	Parkinson's Disease
PET	Positron Emission Tomography
Pi	inorganic Phosphate
ROS	Reactive oxygen species
T	Tesla
T1	Longitudinal relaxation time
T2/T2*	Transverse relaxation time
TE	Time for Echo
TR	Time to Repetition

Acknwoledgements

I would like to thank our funding agencies, CFI and CIHR that have provided the resources without which the project would have never seen light.

This project is above all a collaboration effort between the LINEV laboratory, and all it's members, CHUM made possible by a research agreement with Siemens that have provided all the resources we requested.

I would like to name and thank the key players of this project, who have helped me;

Gilles Beaudoin from CHUM,

Raphaël Paquin, from Siemens,

Rick Hoge from LINEV and my research director.

To you, thank you for your mentoring and guidance.

To my friends and colleagues from LINEV that have helped through better and bad results, Claudine Gauthier, Cécile Madjar, Isabelle Lajoie, Élodie Boudes, Anne-Marie Bédard, Tairk Hafyane, Felipe Tancredi, Paul_Olivier Leclerc and Sébastien Proulx, thank you for your help, your time and your efforts, the dances and the good times.

To the UNF that have trained me, Francine Bélanger, Carollyn Hurst, André Cyr and Julien Doyon, thank you for you support, discussions and help.

Finally, thanks to my family, who shall never really understand this project completely, but tried hard and supported me nonetheless.

Introduction

In several pathologies, visible anatomical changes are driven by metabolic changes. In the case of liver tumors in the mouse model, tumors growth and regression have been shown to occur after changes in aerobic glycolysis and oxidative phosphorylation (Hu et al. 2011). In such work, the tumor's growth appearing after a switch to a different metabolism pathway and its regression occurring after regression to the original metabolism, confirms the existence of two metabolic states with their own specific anatomical expression. This confirms the possibility of using metabolism as an early predictor for pathology.

Altered metabolisms have also been observed in humans, during the early stages of Alzheimer's disease (AD) for example (Martin 2007). In the model used to describe the AD cascade (Jack et al. 2010), first Aβ-plaque deposition and then glucose utilization observed under FDG-glucose PET (positron emission tomography) precedes the changes visible in anatomical MRI(Mosconi et al. 2010). Reliable measurement and monitoring of theses changes in metabolism are of growing interest in the community and are the key to understand and prevent evolution of MCI (mild cognitive impairment) patients towards fully developed AD. Although PET is the gold standard when it comes to observe metabolism, MRS (magnetic resonance spectroscopy) can offer an alternative that doesn't require the use of radiation.

However, MRI scanners do present a challenge; few come with out-of-the-box solutions for metabolism imaging, and a large effort in coil development, sequences and debugging needs to be brought together for their implementation. Although it sounds cost prohibitive, it opens new avenues that add significant value to ongoing research on energy metabolism and its use in the human body. This is why we decided to develop the necessary tools and expertise in MR phosphorus spectroscopy.

In this work, the reader will find the various design steps that were taken towards developing a working single loop coil tuned to the phosphorus resonance with specifically made phantoms. As the first steps for further projects it also explains future

designing iterations and possible applications in research in a near future.

The next chapter will present a brief overview of brain metabolism as it is understood and will identify the key metabolites that can help monitor this metabolism. Then, the best know technique to measure these metabolites is going to be presented.

Chapter 1: Physiology

The body uses chains of carbohydrates, or fuel molecules, as substrate to create high energy transport molecules like ATP. These high-energy molecules are used throughout the body to maintain the metabolic activity. This energetic metabolism is vital to our organism and can be broken down in to three stages; glycolysis, Krebs cycle, and electron transport chain(Vander Luciano and Fox 1992). In the next chapter, a description of where and how theses processes occur will be done. If the energy utilization in the muscles is fairly well understood, is it not the same for the brain. A brief discussion will give an overview of the modern ideas in the literature over the coupling between neuronal activation and its energy-demand matching.

From glucose to ATP

The main fuel for energy in the human body is glucose. This molecule is stored in the liver and slowly released in the blood stream to keep its concentration constant. The first stage of energy molecules genesis is glycolysis in witch glucose will be degraded into pyruvate and ATP. This mechanism requires 2 molecules of ATP to be invested that will be recovered the end of this first phase. The following diagram details the ten steps enzymatic mechanism of this cytosolic pathway.

This transformation is possible because of the presence of ATP that acts as a catalyst for this chain of reactions. Although it is not clear from the diagram, these reactions are in fact dynamic equilibriums and the creation of pyruvate stops when its concentration is too high. Reaction 4 creates two isomers that can undergo the same metabolic pathway, this means that products from reactions 6 to 10 are actually doubled for a net gain of 2 ATP per glucose consumed. Lastly, it is worth mentioning that this entire process is self sufficient and no other input than glucose and catalytic ATP are required. This chain of reaction can be performed in both aerobic and anaerobic environment and this is why it is the basic energetic pathway for organisms, even primitive ones like yeast.

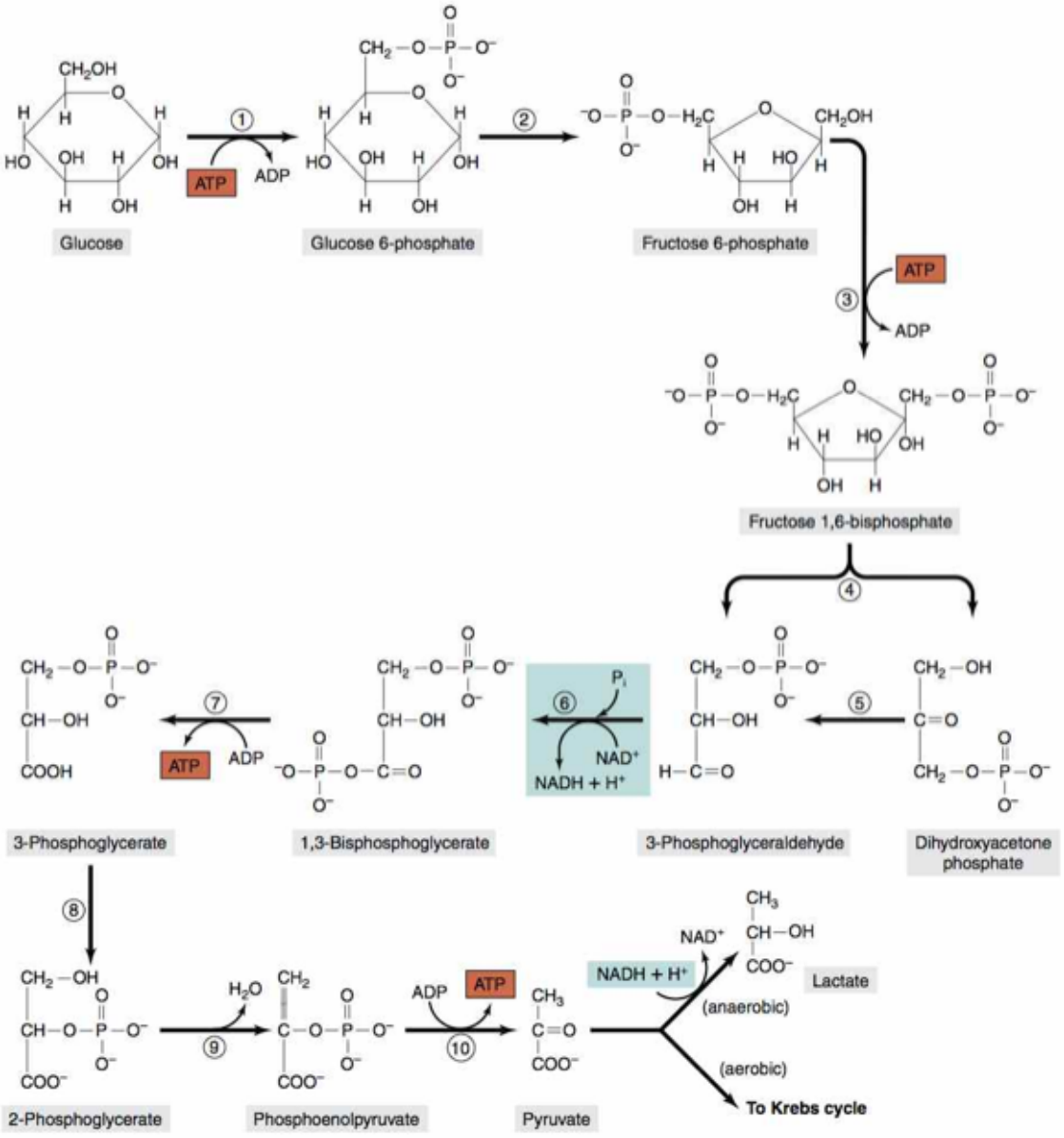

Figure 1 - **Glycolysis diagram, as seen in Vander's Human Physiology.** (Vander Luciano and Fox 1992)

If anaerobic organism like yeast are producing lactate as their final product, the addition of oxygen as input bring the second phase of this process, the Krebs cycle.

This cycle uses the pyruvate created in the previous phase as a catalyst. Together with coenzyme A (CoA) it creates the precursor Acetyl-coenzyme A that is the entry molecule of the cycle and CO2 that will be the first by-product. During the cycle, the addition of the two carbon atoms attached to acetyl-CoA will be cancelled out by the elimination of two other carbon atoms in the form of additional CO2 molecules. In the

next diagram, this is represented by reactions 3 and 4. Reactions 5 to 8 are simple rearrangements to be able to accept a new acetyl-CoA molecule and repeat the cycle. Unlike glycolysis that takes place in the cytosol, the Krebs cycle, and the oxidative phosphorylation after, take place in the inner membrane of the mitochondria. This proves to be useful because both of theses last stages are actually coupled.

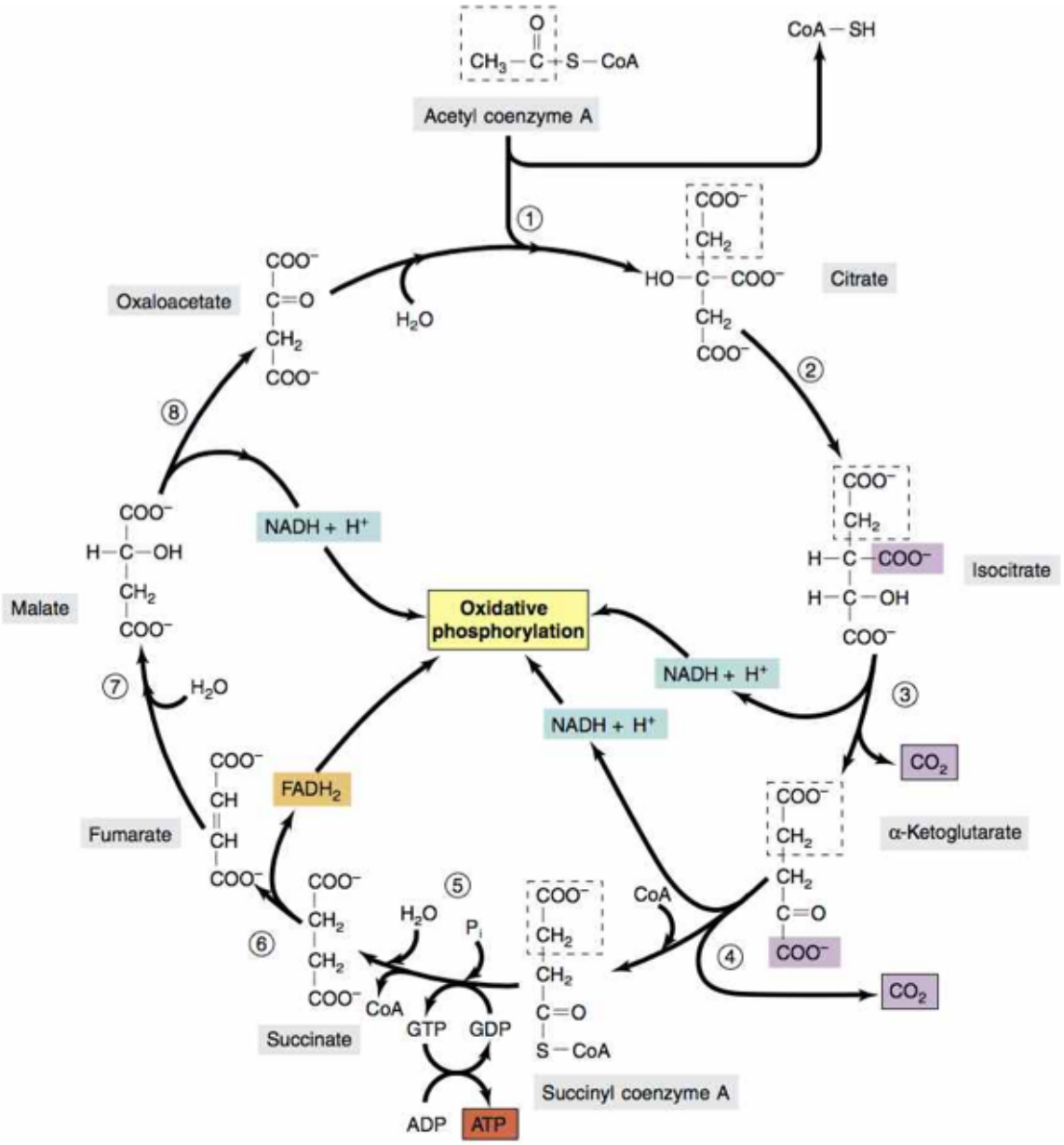

Figure 2 - Krebs cycle diagram, as seen in Vander's Human Physiology. (Vander Luciano and Fox 1992)

From the previous diagram it would appear that this stage doesn't require oxygen, but the Krebs cycle needs to regenerate the NAD+ and FADH coenzymes that are

necessary to evacuate the hydrogen atoms, liberated together with CO2 molecules, in the form of NADH and $FADH_2$. This regeneration takes place during the last oxygen consuming stage: the oxidative phosphorylation.

This last stage is the one that consumes one molecule of oxygen and creates two of water. To do so, it regenerates the coenzymes NAD+ and FADH liberating H+ ions and free electrons pairs. The elevated H+ concentration inside the mitochondria create an electric potential that assures the function the ATP-synthase pumps that are going to evacuate one H+ ions back to the cytosol and link one inorganic phosphorus atom with ADP to create one molecule of ATP.

The following diagram shows the oxidative phosphorylation (complex IV and ATP synthase).

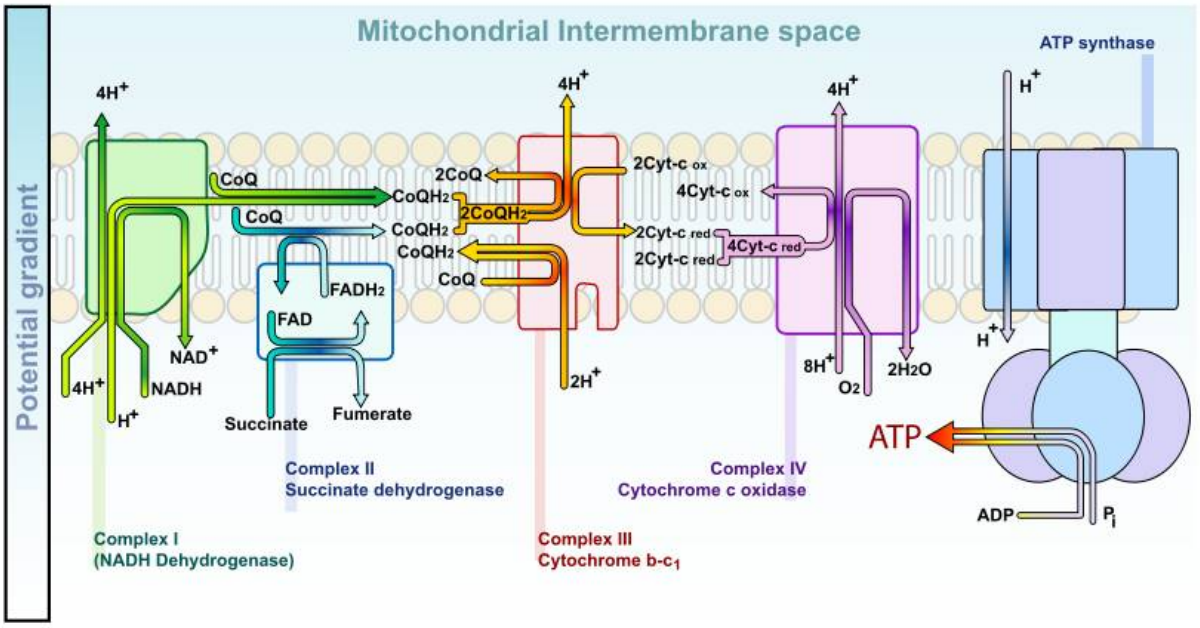

Figure 3 - Mitochondria inner membrane complexes participating in ATP generation. As found in :http://hepato-neuro.ca/uploads/images/contenu/ETC_electron_transport_chain.jpg

The previous paragraphs explain how glucose can be degraded to into CO2 and H2O to create ATP. The overall reaction can help create a total of 38 molecule of ATP under aerobic conditions, compared to the only 2 ATP under anaerobic conditions like in yeasts. This entire process can be summarized in the next diagram.

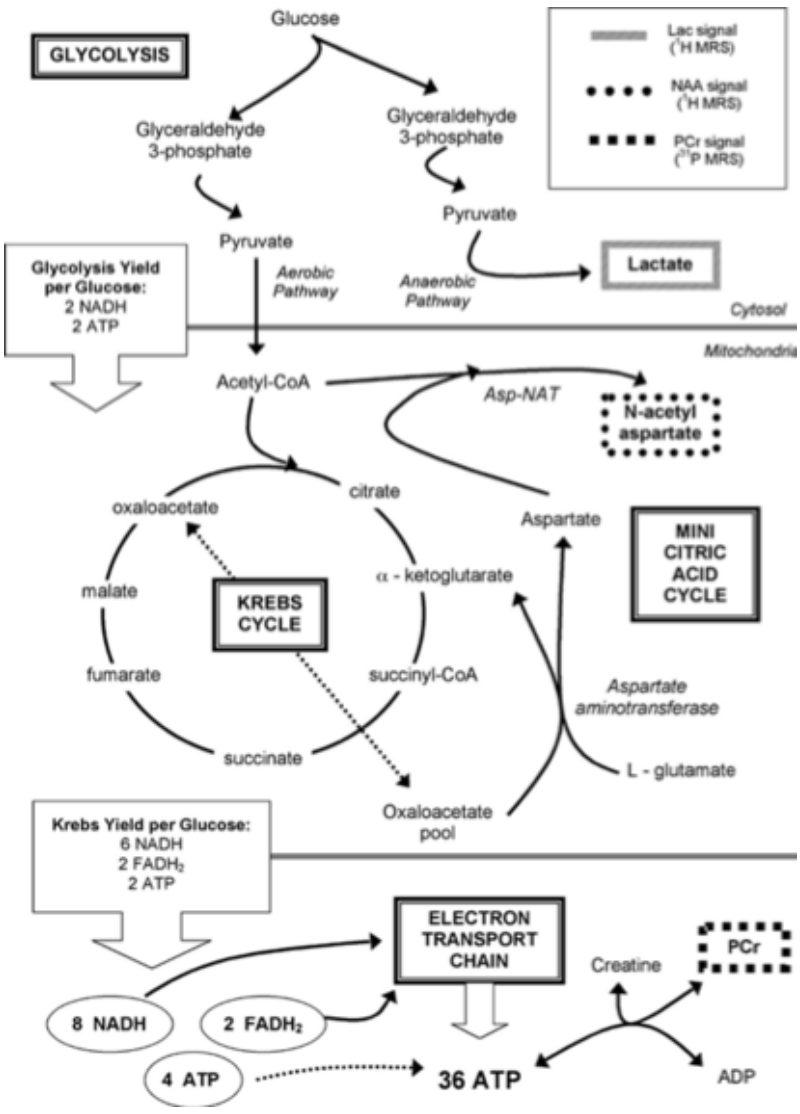

Figure 4 - Overall generation of ATP through breakdown of glucose via glycolysis, Krebs cycle and oxidative phosphorylation. (Stork and Renshaw 2005)

Energy in the muscles

ATP is an energy vector in the human body. In muscles, the high-energy phosphorus bound is however stored in creatine, in the form of phosphocreatine. It is found in the cytosol, and serves as a pool of stocked energy readily available on demand. For short and powerful exercise, the phosphocreatine pool depletes its self to regenerate rapidly the ATP needed for muscle contraction. With enough oxygen in the blood stream, it is also possible to regenerate ATP form ADP through the oxidative phosphorylation. Both mechanisms are balanced to keep the ATP levels constant.

However, when the workload increase over the oxygen capacity, ATP is consumed without complete regeneration, and the fermentation process follows the glycolysis, creating accumulations of lactate in the cytosol. Lactate will decrease local pH, and will need to be transformed to pyruvate or evacuate from the cell through blood flow. Phenomena such as acidic cramps are attribute to excessive local lactate, although recent findings attribute the cytosol acidification to inorganic phosphate also(Westerblad, Allen, and Lännergren 2002).

With the previous description of the energy metabolism, it is possible to see that lactate is only one by-product of intense work from the muscle. To get more precise understanding of the metabolism, phosphorus imaging can help quantify variations in ATP and phosphocreatine. Proton MRS gives only a partial view where as phosphorus MRS can give richer information on the same metabolism. If many studies have looked into the proton and phosphorus metabolism of muscles and found similar conclusions, energy utilization in the brain still poses some unanswered questions and tapping into mitochondrial metabolism could help understand some of the dysfunctions observed, notably in aging.

Applicable research areas

The brain activation and energy consumption

Energy utilization in the brain has not been as widely investigated than in the muscles. From previous models based on single cell analysis, where each neuron creates its required energy, a more complex model has evolved where neurons and astrocytes are couple in their energy production, the later acting as production and storage area for the former(Bélanger, Allaman, and Magistretti 2011).

Since the discovery of the uncoupling between cerebral blood flow (CBF) and cerebral metabolic rate of oxygen (CMRO2) (P. T. Fox and Raichle 1986), it has been accepted in the scientific community that brain metabolism is not (or not completely) explained by a purely oxidative metabolic pathway. The astrocyte lactate shuttle model, proposed by Pellerin (Pellerin et al. 1998), was tested by a number of MRS experiments

that proved the importance of lactate as an immediate substrate for energy during visual stimulation(Magistretti and Pellerin 1999; Mangia, Tká, et al. 2007; Mangia, Tkác, et al. 2007).

Much work still needs to be done to fully understand the part of each compartment in the brain and the various fluxes and signaling between them. Nevertheless, it is possible to say that both oxidative and non-oxidative glucose transformation to energy occurs as described earlier.

Energy metabolism and aging

In the past years, mitochondrial dysfunction was put at the heart of the debate in aging diseases. Authors have succeeded to correlate neurodegenerative disease like Alzheimer's and Parkinson's disease (PD) to alterations in the mitochondrial functions(Wallace 2005), (Piaceri et al. 2012).

From the electron transport chain, several harmful by-products can accumulate in the mitochondria. These by-products, named reactive oxygen species (ROS) are known to interact strongly with DNA and proteins from the electron chain complex. Anti-oxidant based defense mechanisms of the human body are in place to prevent this self generated attack, but they prove less and less effective over time. When the ROS concentrations are too high to be match by the defense mechanism, oxidative stress occurs(Wallace 2012).

The markers of oxidative stress have been correlated to neurodegeneration, like in AD or PD. These mitochondrial dysfunctions are visible on MRS measurements for both diseases.

Using proton spectroscopy, it is possible to show decreases in Naa/Cr ratios, explained by slowed genesis of Naa in the mitochondria with PD patients(Clark 1998).Theses results correlate with findings using phosphorus spectroscopy where reduced metabolism observed via Pi/PCr (inorganic phosphate/ Phosphocreatine) ratio is explained by destruction of the Complex I in the oxidative phosphorylation in patients affected by PD(Gu et al. 1998). This mitochondrial dysfunction appears to be widely spread throughout the body.

In the case of Alzheimer's patients, accumulations of phospholipids can be

observed using 31P spectroscopy. Both phospho-mono-esters and di-esters of the cell's membrane are visible using 31P MRS(Wijnen et al. 2010), but further studies are needed to clearly understand the process of this accumulation. Under proton spectroscopy, affected neurons integrity is visible by localized lower Naa/Cr ratios.

Close understanding of mitochondrial functions in the brain may prove very important in research on AD and PD, and tools to quantify mitochondrial energy production should be used when looking for specific markers of these disease.

From the previous paragraphs, it is possible to understand that brain metabolism is still a black box in which possible pathways are known, but their compartmentalization and quantification still poses real challenges to researchers.

The urgency of solving brain metabolism is even more understandable in a context where tremendous efforts are made toward explaining and preventing AD and PD in our aging populations, for which mitochondria dysfunction has taken a central position.

Among the various approaches to probe the energy metabolism, MRS proves to be a non-invasive and quantitative tool for researchers. The following aims to make an overview of the implementation of such tool.

Chapter 2: Physics of magnetic resonance

The following chapter will explain the origin of the magnetic resonance phenomena and how it is apply in MR imaging and spectroscopy. Recording of images and spectrum will be detailed as well as the importance of using various sequences.

Description of magnetic resonance

Microscopic scale

Magnetic resonance uses the intrinsic susceptibility of nuclei that presents a spin different from 0. The distributed charges of their nucleus, rotating on its axis are the equivalent of a single charge in constant movement along a circular orbit.

From classical Physics, it is possible to describe the magnetic moment create by a rotating charge about an axis using the following equation, where μ is the magnetic moment, γ the gyromagnetic ratio and L the angular momentum vector:

$$\mu = \gamma L \qquad [1]$$

γ is dependent on the nature of the charge and can be calculate using the following equation, where e is the charge and m its mass:

$$\gamma = (\frac{e}{2\pi}) \qquad [2]$$

On the other hand, L describes the rotation movement with the equation below, where r is the distance to the center of rotation, and v the velocity:

$$L = r \times mv \qquad [3]$$

In the case this rotating charge is placed in a magnetic field B_0, a torque T will be

applied to the loop around which the charge rotates.

$$T = \mu B_0 \leftrightarrow \frac{d\mu}{dt} = \gamma \mu B_0 \qquad [4]$$

This last equation illustrates the change in orientation of μ relative to B_0 i.e. the precession of μ about B_0. This equation is called the Larmor equation, and has the following usual form:

$$\omega_0 = \gamma B_0 \qquad [5]$$

From this equation, it is possible to isolate the Larmor frequency, which will be useful in the next paragraphs.

$$\upsilon_L = (\frac{\gamma}{2\pi})B_0 \qquad [6]$$

It is possible to calculate, using previous the equation, the resonance frequency of specific atoms, which depends on its gyromagnetic ratio and the field strength.

Table 1 - Resonance frequencies for proton and phosphorus using Siemens Tim TRIO 3T (actual field: 2.89T).

Table 1 - Excitation and relaxation of magnetic moment

Atom	Gyromagnetic ratio (MHz.T^{-1})	Resonance frequency at 2.89T (MHz)
Proton (^{1}H)	42.58	123.06
Phosphorus (^{31}P)	17.235	49.81

From the equation described above, it is possible to describe the rotation of the magnetic moment in a constant magnetic field B0 using an orthogonal system where one axis Oz has the same direction as B0 and a normal plane xOy rotating at frequency ω0. In such system, the first equation becomes:

$$\mu_z(t) = \mu_z(0) \quad [7]$$

$$\mu_x(t) = \mu_x(0)\cos(\omega_0)t + \mu_y(0)\sin(\omega_0)t \quad [8]$$

$$\mu_y(t) = \mu_y(0)\cos(\omega_0)t - \mu_x(0)\sin(\omega_0)t \quad [9]$$

If another magnetic field B_1 is applied to the system, the previous equation becomes:

$$\frac{d\mu}{dt} = \gamma\mu B_0 \rightarrow \frac{d\mu}{dt} = \gamma\mu(B_0 + B_1) \quad [10]$$

The next section will explain how this additional field is created. The B_1 field is usually a radio frequency rotating field normal to the Oz axis, which will keep the magnetic moment rotating around its Oz axis, but bring it form a parallel alignment to a perpendicular one. The duration and intensity of the B_1 excitation will need to be calibrated and will give the angular offset created from the parallel direction.

For MRI and MRS applications, typical offsets of 90° and 180° are used to bring the magnetization from parallel to perpendicular orientation or to switch it from parallel to anti-parallel. Sequences use variations on theses offsets and their timing to create the appropriate contrast desired.

After excitation, the main field B_0 drives the magnetic moment back to its original precession. It is then that the MR signal is received. A coil measures the magnetic component in the orthogonal plane to the B_0 field. When the magnetic moment rotates in the orthogonal plane, under constant B_1, the current create in the RF coil is similar to a sine wave. When B_1 disappears, the envelop of this sine wave decrease exponentially. It is called the relaxation.

It is important to know that the bulk magnetic moment created arises from few atoms in a million and that is why the measured signal is so low. This susceptibility is

even lower when imaging phosphorus atoms, and more signal needs to be recorded, by averaging or taking larger voxels.

While classical physics let us understand how to manipulate a magnetic moment with magnetic fields, the relaxation phenomenon is driven by interactions with the nuclei described as described by Bloch.

The Bloch equations

Lets define M as the bulk magnetic moment. The Bloch equations let us understand the dynamic with which the relaxation occurs. Under constant B_0, M_z, or the Oz component of M, is constant and equal to M_0. After excitation the first Bloch equation describes the spin-lattice relaxation, or longitudinal relaxation as follow:

$$\frac{dM_z}{dt} = \frac{M_0 - M_z}{T_1} \qquad [11]$$

T_1 is a time constant that varies from one material to the other. It describes the energy transfer form the spin to its surrounding.

There also exists a transverse relaxation, or spin-spin relaxation that represent the decrease in net magnetization in the transverse plane due to exchanges of magnetization from one spin to the other. This relaxation is a loss of phase coherence from the magnetic moments, and this relaxation can be described by T_2 as follow:

$$\frac{dM_x}{dt} = -\frac{M_x}{T_2} + \gamma M_y B_0 \qquad [12]$$

$$\frac{dM_y}{dt} = -\frac{M_y}{T_2} + \gamma M_x B_0 \qquad [12]$$

In reality, additional microscopic changes in B0 homogeneity contribute to this relaxation and T2*, effective T2, is the time constant that describes transverse relaxation.

$$\frac{1}{T_2^*} = \frac{1}{T_2} + \frac{\gamma \Delta B_0}{2} \quad [13]$$

The transverse relaxation can be used to boost the MRI signal. If a spin system was allowed to go out of phase for a given time *x*, applying a 180°excitation pulse will invert the magnetization and spins will return progressively in phase. After the same *x* amount of time, it is possible to measure this *echo* with maximum signal minus losses due to field inhomogeneity. This is particularly useful in sequences design.

Application: MRI and MRS

The previous section presented the physical principles behind magnetic resonance. The next section will explain the implementation steps necessary to conduct meaningful MR experiments.

The MR system

From the equations above, the necessity of a strong magnetic field is mentioned. This magnetic field exists continuously in the bore of MRI scanners. They are classified by the strength of their magnetic field, measured in Tesla, where 0,5-1,5T is low and the most clinically available, and 3T is considered high. New scanners around the world are being built with up to 11T for research on humans and even larger fields for animals studies.

Scanners are also equipped with gradients that are designed to alter the magnetic field locally. Their arrangement is so that it can create linear variations of the magnetic field in all three directions of space. The following figure gives such arrangement. These gradients are used during localization to perform slice selections that are going to be detailed in a later section.

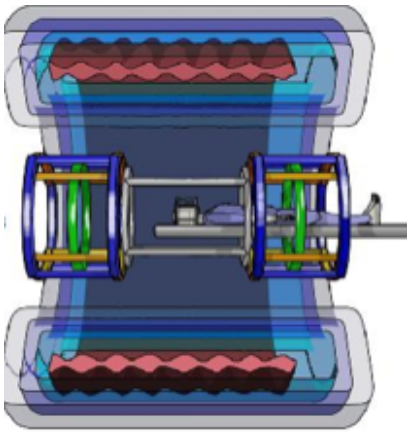

Figure 5 - Gradient coils arrangement for field manipulations in 3 orthogonal directions. (Hoa 2007)

The last elements needed are the coils used to transmit and receive the radio-frequency energy to and from the sample. Although the MRI scanner does have an internal coil tuned to the proton frequency, called the "body-coil", additional coils, put closer to the object of interest, specifically tuned and shaped may be used to increase the signal to noise ratio. Since the project at hand involves iteration on coil design and calibration, much information will be given through out the next chapters about them.

To orchestrate all three elements mentioned together, the MR technician uses a computer that will control the amplifiers for gradients and radio-frequency emitters. The computer is also responsible for data collection from the receiving coils, some post processing and image display.

With a better understanding of the MR system, it is now possible to take a look at a standard acquisition protocol.

Recording and images

The most basic sequence used for imaging is called "spin-echo". It consists of two RF pulses excitation in the presence of gradient variations. The first pulse, creates the transverse magnetization, the second the refocusing of the signal to create the echo. The gradient in the Oz direction during excitation make it possible to select only one slice at the time, since the resonance frequency then becomes position-dependent on the Oz axis. The signal positioning in the selected slice is encoded using the phases and frequency

gradients. After encoding, spins are excited with a 180° pulse to create the echo.

The images created are 2D Fourier transformed and may need some post-processing before analysis.

Sequences are characterized by their TR (time before repetition, between two excitations) and TE (time before echo). These tow parameters can be tuned to maximize desired contrast. A T1 weighted image will use short TR and TE to differentiate tissues on their longitudinal relaxation. On the opposite, a T2 weighted image will use long TR and medium TE to differentiate tissues on their transversal relaxation. A third contrast, called proton density, uses short TE and long TR to image the density of reactive spins in a given slice.

Spectroscopy and Fourier Transform

Imaging sequences create a spatially encoded image of the intensity of the signal, whereas spectroscopic sequence focuses on a single voxel, creating an echo signal to be analyses in the frequency domain. The easiest sequence that can be performed is the un-localized free induction decay, or FID. After a typical 90° excitation, it measures the signal's decay. A 1D Fourier transform of this signal gives the frequency signature of the sample. The following figures give the free induction decay component of M_x and M_y over time, and the results of its Fourier transform.

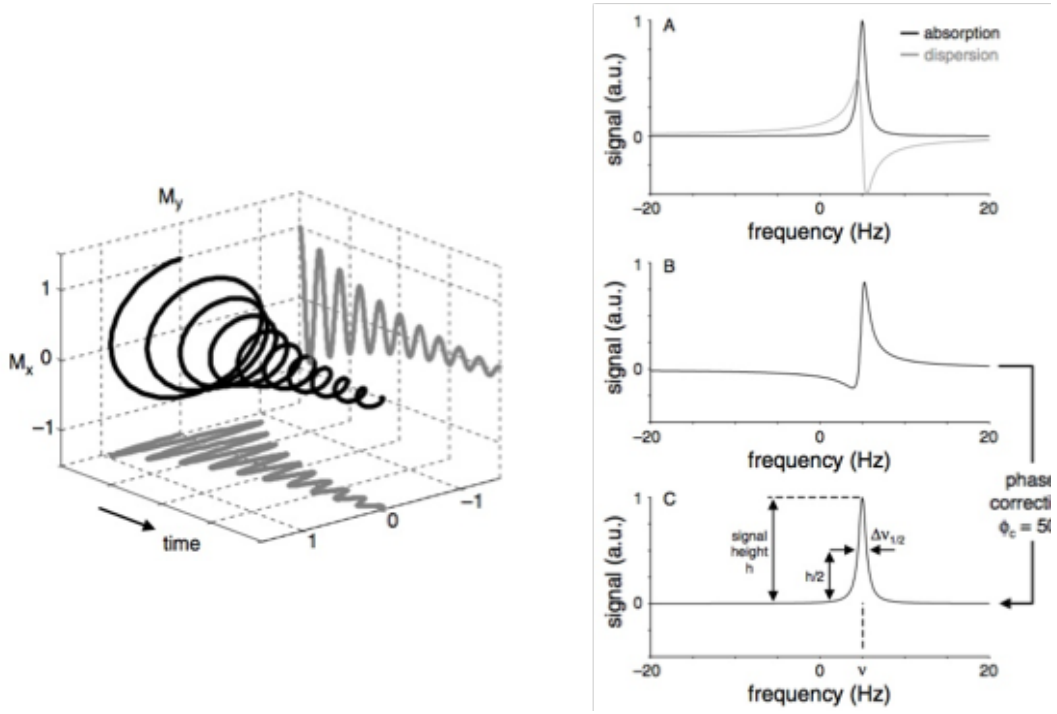

Figure 6 - Exponential decay of Mx and My, and its Fourier transform. (De Graaf 2008)

Chemical shift

Because of the electromagnetic field created by the electrons, each atoms susceptible to react to NMR experiment is somewhat shielded by its surroundings. For each atoms with similar surroundings, it is possible to described the visible magnetic field as follow, where σ is the shielding constant:

$$B = B_0(1-\sigma) \qquad [14]$$

Because each nucleus has a specific σ related to the surrounding, (for example, the presence of oxygen instead of carbon as a neighbor) its resonance frequency will differ slightly. The exact frequency becomes:

$$\omega = \gamma B_0(1-\sigma) \qquad [15]$$

Because these variations are very small, it is commonly expressed in unit-less δ part

per million, where ωref is the resonance of a chemical reference:

$$\delta(ppm) = \frac{\omega - \omega_{ref}}{\omega_{ref}} 10^6 \qquad [16]$$

For proton spectroscopy, the reference is TMS (tetramethylsilane), with 12 equivalent 1H nuclei, and water is the strongest peak resonating around 4.7ppm. For phosphorus spectroscopy, the reference is phosphocreatine (PCr), the strongest peak in the spectrum.

Chemical shift not only let us identify nucleus from different environments, but also quantify the number of similar environments, since the area under each peak is proportional to the number of nucleus for this surrounding.

J-coupling coupling

In some more complex cases, peaks are split because of energy transfers between nuclei of the same system. This interaction is named J-coupling, or scalar coupling.

When two nuclei, like 1H and 13C are bound by sharing their electrons, the spin orientation of the later is opposite to one another, and the energy ΔE needed to switch form one orientation to the next will be proportional to the nuclei's Larmor frequency.

In the presence of interaction between nuclei via their electron cloud, the Pauli exclusion dictates that theses electron should have opposite spins, to minimize the energy of this bound. The transition energy equation will be altered by a coupling constant J. There now exists two resonance frequency for the same nuclei separated by J Hz.

$$\Delta E = hf_{ref} \rightarrow \Delta E = h(f_{ref} \pm \frac{J}{2}) \qquad [17]$$

In highly complex spin systems successive splitting occurs, following a Pascal

triangle. If singlet and doublet are analyzed, spin systems that give rise to more complex signatures like quadruplets are usually not taken into account because of the low resolution and high noise level of spectra.

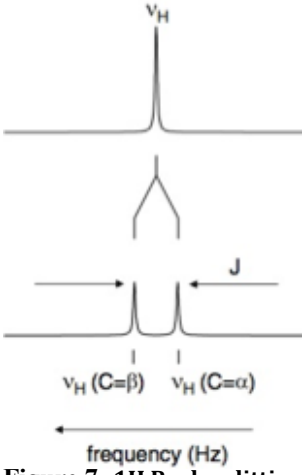

Figure 7 -1H Peak splitting, in presence of J-coupling with 13C atom. (De Graaf 2008)

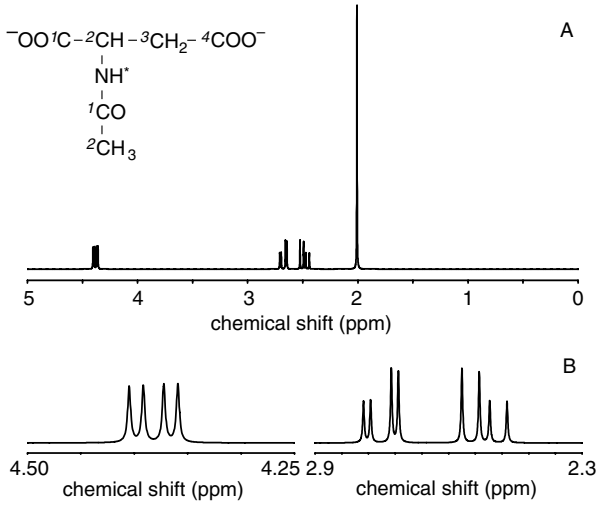

Figure 8 - MR Spectroscopy signature of NAA, resonance for CH and CH2 are usually ignored. (De Graaf 2008)

Sequences

In practice, the FID is not widely used. Instead, localized sequences like PRESS or STEAM are preferred.

Press sequence

Point-resolved-single-voxel-spectroscopy, or PRESS sequence, is the most basic localized spectroscopic sequence. The following figure gives a time representation of this sequence.

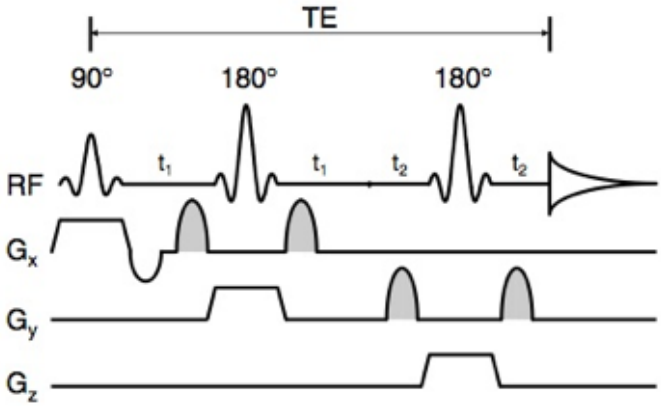

Figure 9 - PRESS sequence. (De Graaf 2008)

In this sequence, two 180° refocusing pulses are used in orthogonal directions to the first pulse so that the generated echo arises from a single localized voxel. The first pulse excites a slice of the volume, the next isolates a strip on this slice and the last, a bloc on the strip. For each pulse, the corresponding gradient is used to select the specific position and width of the voxel in the volume. The TE is the time between the first pulse and the acquisition. Gradients in gray are used to spoil unwanted signal.

Steam sequence

Another widely used sequence is the STEAM sequence. Like the PRESS sequence, it uses three orthogonal RF pulses to create spatial localization. Each pulse will create an echo but the strongest one will be STE the echo that appears TE+TM time after the first excitation. Using gradient crushers it is possible to null the other echo.

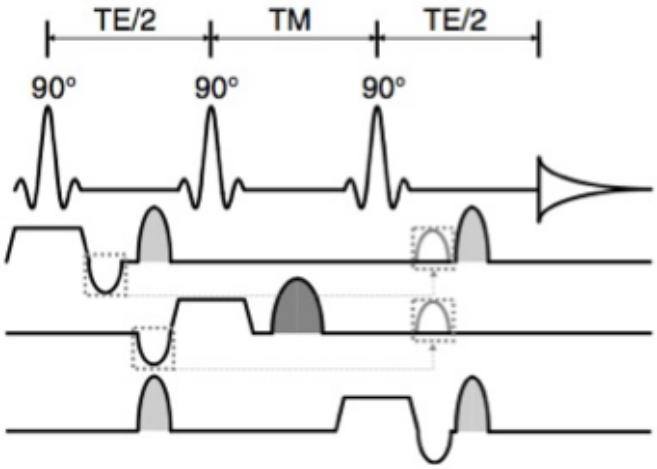

Figure 10 - Steam sequences echos. (De Graaf 2008)

This sequence is particularly useful because it not only localizes the signal, but it is possible to exploit the TM dependence of certain metabolites to get stronger signal.

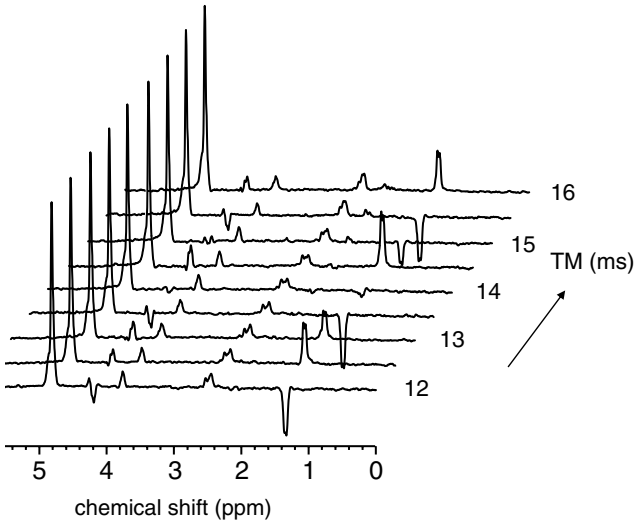

Figure 11 - **TM dependence of Lacate and Glutamate at TE=144ms.** (De Graaf 2008)

These sequences are very interesting and simple to use, but they are limited in their lowest TE by of the length of the RF pulses and the gradient rising time. In proton spectroscopy, the challenge is to find the right TE and TM for the best contrast of the molecules to be imaged. In phosphorus spectroscopy, the amount of signal available makes the challenge of limiting the TE to its lowest value possible while using

localization RF pulses.

This chapter presented the various concepts to explain MR experiments and how images are formed. It also explained how MR spectroscopy experiments are used to isolate metabolites frequency signature and different sequences are used to localize and contrast these signatures. Because the challenges in proton spectroscopy are different than the ones in phosphorus spectroscopy, the proposed solutions must be different from one to the other. In the next chapter, we will expose some of theses challenges and why phosphorus spectroscopy can yield rewarding results.

Chapter 3 : From proton to phosphorus imaging

In the previous chapter, the MRI and MRS techniques have been explained. If hydrogen atoms give a relatively strong signal, it is sometimes not appropriate for MR experiments, and other nucleus need to be studied. The next chapter will present the inadequacy of proton spectroscopy at 3T when studying the energy metabolism and will give an alternative: phosphorus spectroscopy.

MRS of Lactate to image metabolism

From chapter 1, the metabolite that is of key interest in metabolism studies using MRS is lactate. Lactate is a small molecule that has two resonances in MRS: its main peak, a doublet at 1.33 ppm, and a quartet around 4,11ppm. The later is usually invisible in *in* vivo studies for it is below the noise level.

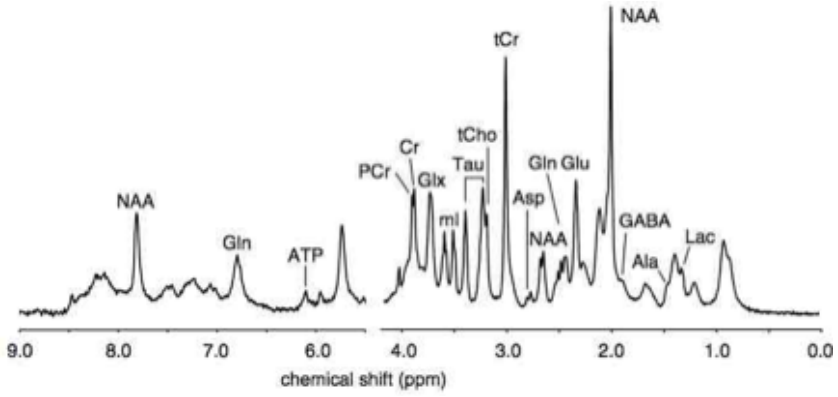

Figure 12 - **Typical 1H MR brain spectrum.** (De Graaf 2008)

Lactate is a difficult metabolite to image(Lange et al. 2006). Not only does it have very low signal because of its low concentration, its main peak sit directly over a large baseline distortion due to lipids and macromolecules. Finally, its signal is nulled at an echo time of 144ms, due to its relaxation properties.

Different adjustments can be made to get reliable lactate measurements *in vivo*.

- First, one can use a shorter or longer echo time; 288ms has proven to give good reliable signal. Using long TE's can also help in reducing the lipid contribution around 1.33ppm. The tradeoff is that the longer the echo time, the smaller the

echo is for each metabolite.

- To avoid baseline distortion, one can pay particular attention to voxel positioning, placing it as far as possible from lipid tissues using an anatomical reference image. Rotation of the voxel of 180° can help, especially with non-ideal slice selection.
- Additional inversion pulses or more specialized sequences like MEGA-Press can help provide more reliable measurement of lactate.

When applying from some to all of theses techniques to acquiring lactate spectrum, it is possible to get a reliable estimate of the lactate concentration of a voxel, but it might take time to get a strong enough signal. It is far from the time resolution needed to observe the dynamics that can be observed with fMRI, or ASL data. Finally this gives access to a limited picture of the underlying metabolism, quantifying only one actor.

Phosphorus MRS alternative

Another approach is to measure phosphorus metabolites using MRS. The reason it is not common practice to do so is that is requires a large investment in implementation and very few clinical applications have been derived so far. In terms of hardware, one must have a multi-nuclear scanner, which is more expensive and fewer institutions are equipped with. Special coils must be purchased or developed to image these new nuclei since scanners are usually delivered with body coils and a series of coils for proton imaging only. Then one must calibrate and test those coils using phantoms that have to be made or purchased through the scanner vendor or a third party. Finally sequences are also usually optimized for proton and must be adapted and tested.

If the implementation cost is prohibitive due to the high price of the multi-nuclear hardware, multinuclear scanner give access to a complete different view of the human body when using magnetic resonance. If all of the above are brought together, it is possible to perform phosphorus spectroscopy and benefit from its advantages.

- Phosphorus spectroscopy is richer in energy metabolite information. It can give

quantification of phosphocreatine (PCr, energy reserve in the cytosol), ATP (readily available energy transport), inorganic phosphate (Pi) and other highly energetic molecules with phosphorus bound, all at the same time.

- Phosphorus spectra are less dense than proton ones for fewer visible molecules contain ^{31}P atoms. There is no baseline distortion from macromolecules and lipids and there is very few overlap between peaks, which makes it easier for quantification.

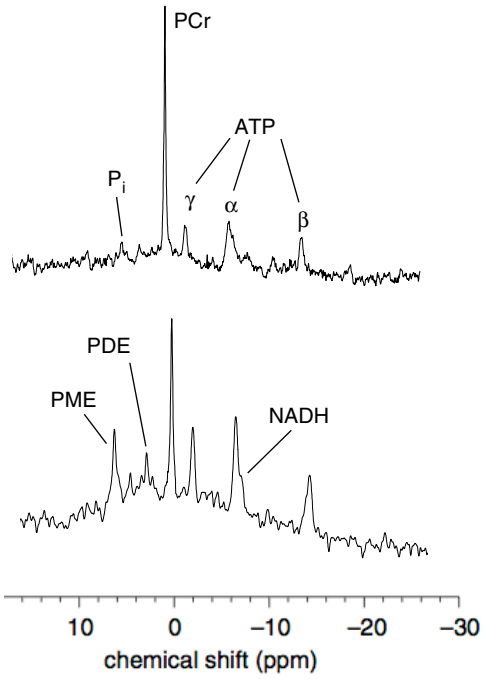

Figure 13 - Typical 31P MR spectrum of a muscle (top) and brain (bottom). **(De Graaf 2008)**

- Finally, it is possible to get good relevant information with relatively basic sequences, like unlocalized *fid. This can prove useful when trying to image dynamic processes of the same time frame than fMRI, namely the neuron activation-BOLD coupling.

These reasons were the ones that convinced us to develop phosphorus capabilities at the research center. It is to be noted that using phosphorus as the resonating nucleus doesn't presents just advantages, but also many challenges. First, the signal decreases much faster than with proton. TE's are generally much smaller, around 20ms or less. Sequences need to adapt, and special localization schemes must be

adopted. The other option is to use unlocalized sequences, when possible.

There is also great improvement to the signal analysis when decoupling is applied. The key is to use saturation RF pulses to null visible exchanges of energy between linked nuclei. This exchange of energy between excitation and acquisition will result in peak splitting and will add overlapping and complexity to the signal.

Phosphorus coil design and implementation

The goal of the project at hand is to be able to measure phosphorus spectra in the human body. There are five steps required to achieve this goal :

- Design and build a coil tuned to phosphorus frequency

- Interface the coil with the 3T clinical MRI system

- Code new sequences adapted from the ones available form proton to meet specific imaging needs

- Design and build phosphorus phantoms to be used as test objects to test the new hardware and software developed for the project prior human testing

- Test the hardware and software on both phantoms and human subjects using new protocols approved by the local ethics comity.

The following chapters will explain each steps of this adventure. First let us describe the coil prototyping.

Chapter 4: Coil design

At the time of experiment, Siemens Healthcare didn't provide commercially available coils for various nuclei, other than proton, at 3T. Such coils need to be either bought from a third party or specifically developed in house. It has been decided that the UNF would build its own set of coils and therefore develop expertise needed for further projects.

Steps to a working design

It has been planned for a volume coil to be developed for localized cerebral studies, but the first step was to prove the feasibility of building a surface coil that could be used for brain studies, but also for muscles. The most basic design was composed of a single loop coil for excitation, with a diameter of 6cm, and a second coil for reception with a diameter of 10cm. The following illustration shows the schematic of these two coils. The separation of the two coils at first, proved helpful to isolate possible problems from transmission and reception of the signal. Both coils are needed to create an image since the internal coil of the scanner (or body-coil) is tuned to excite and receive at the proton frequency only.

Small single loop coil tuned to 31P

Geometry and general aspect

Once working, the two coils were put together on the same plug. An additional electronic filter was added to the design on the receiving end of the circuit to disable it during scouts and anatomical imaging using the proton frequency. The following illustrations show (additional schematics and) a photo of this coil.

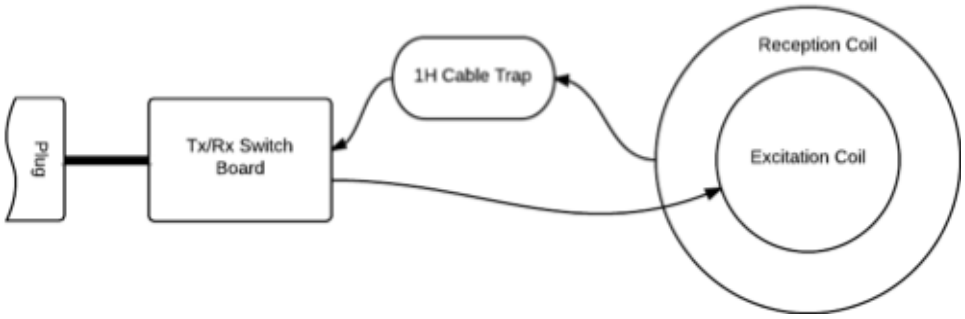

Figure 14 - Schematic of the coil, presenting its four distinct parts.

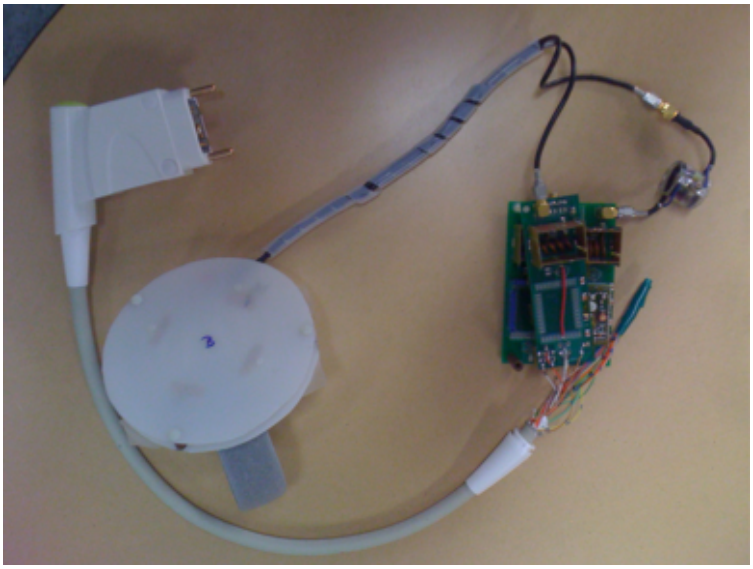

Figure 15 -31P Coil prototype as it was used during calibration, It is possible to identify: the plug, the electronic board for transmission and reception, the proton-trap, and the two-loops plastic enclosure

The plastic enclosure for the loop wires is curved to fit comfortably on someone's calf or head. It is tied to the calf using a Velcro strap to minimize possible signal loss due to movement. The two co-axial wires are kept tight in plastic spring to minimize the area create in between the two, since it can act as an antenna and disrupt the signal.

Transmission voltage calibration

Before using a new coil, a standard calibration procedure to optimize transmission voltage for that coil is performed. This procedure requires to used the *fid sequence with a short TE and relatively long TR while increasing the transmission voltage over a given range. The goal is to find the smallest value of voltage that gives the largest signal response. The expected curve is similar to a sine wave, where signal response first

increases with increasing voltage toward a value V_{critic}, where the voltage used gives a true 90° excitation. Beyond this V_{critic} value, the excitation exceeds 90° and the signal diminishes with increasing voltage. It will eventually reduce to 0 for a value of $V_0 = 2 \times V_{critic}$, for the effective excitation will be 180° and the spins will stay in the same direction acquiring enough energy to transform from parallel orientation to anti-parallel.

For this calibration, two phantoms of 500 mL containing 10mMol and 100mMol of PO4 respectively, were used as well as a subject to which the coil was attached to his calf. These two phantoms are described in chapter 5. All subjects who participated in this project were asked to give written consent as part of the protocol approved by the CRIUGM's ethics comity (CMER-RNQ-11-12-016). For each experiment, the *fid sequence was used with TE= 0.35 ms, and TR= 1500ms. Transmission voltage was increased from 10Volts to 200Volts with 10 volts increments. For each voltage, a number of 10 averages were used to get robust data.

B1 field and coil penetration

The B1 field is generated by the current running in the excitation loop and is added in space to the ever-present B0 field. The Biot-Savart law below can describe this B1 field in space like below.

$$B_0 = \frac{\mu_0}{4\pi} \oint \frac{Idl \times r}{|r^3|} \qquad [18]$$

From this equation it is possible to see that the B1 field's strength is inversely proportional to the cubic power of the distance to the coil r. The excitation is therefore more effective for elements closer to the coil. The receiving coil being wider than the excitation coil, it is expected to receive the signal from the entire excited area and some more. The excitation coil is therefore the limiting component for imaging volume, when using a surface coils.[1]

[1] To be able to image deep structures, like hypothalamus in the brain, volume coils are used.

SNR on images

The signal to noise ratio can be used to assess of the coil's quality, giving a quantitative value of how much signal is being detected over noise. Different equations of SNR exist in literature, and have been tested.

SNR can be calculated from a single image by doing the ratio between the average signals S of the region of interest over the noise level derived form the standard deviation of the background signal N.

$$SNR = S / N \qquad [19]$$

In order to take into account the possible offset, or DC component, this offset can be calculated as the mean signal of a selected background area.

$$SNR = \frac{S - offset}{N} \qquad [20]$$

For this exercise, two FLASH images were acquired. The 64 by 64 matrix represent a field of view (FOV) of 300 by 300 mm with a slice thickness of 100 mm. The resolution was then of 2.13 by 2.13 by 0.01 mm^3. The TE and TR used were 4.8 ms and 100 ms respectively, with flip angle of 10°. These parameters ensure to get relatively good signal without taking too much acquisition time, using only 16 averages.

The two images where acquired one after the other in the same session. Each image was analyzed independently first, then together for SNR calculation.

From each image an ROI containing the pixels with largest signal was drawn. The total signal over this ROI was average to give S. Another ROI of the same size was placed over the background, away from the object imaged. The average of the signal in this second ROI was the offset and the standard deviation of the signal over this same region was the noise distribution N. Using the same approach for the two images, the SNR was

calculated using the two previous equations.

Although this gives a good approximate of the SNR, the NEMA standard was more appropriate for surface coils because of their largely inhomogeneous B1 fields(NEMA 2008).

In absolute value images, the noise distribution is not homogeneous. The distribution is gaussian for signal containing ROIs, and in non-signal-containing ROIs it follows a Rayleigh distribution. Therefore, it is necessary to correct the SNR equation accordingly.

$$SNR = 0.655\frac{S}{N} \qquad [20]$$

In equation 20, the 0,655 factor is the correction factor to apply to take into account the differences in distribution of noise in the image (NEMA 2008). From one of the original images, the mean signal, S is calculated. Then the purely noise image is obtain from the pixel-to-pixel difference image from the two images acquired under the same conditions. The noise level N is defined as the standard deviation calculated form the region where no signal and no artifacts were measured.

For reproducibility purposes, it would be interesting to repeat those measurements under standard controlled temperature conditions, using longer TR and more appropriate FOV and more acquisition averages for better SNR estimates. The NEMA standard offers suggestions on these parameters to compare coils between sites. In the case at hand, the SNR can be used to compare coils performances form one design iteration to the next.

Positioning in the scanner, and proton visualization

When using phantoms, the coil was placed closest as possible to the phantom to be imaged. For each acquisition, the two phantoms were placed one on top of the other, the one of interest placed on top. They were maintained in place by a foam support. Three additional bags of saline solutions were placed around the phantom to approximate the loading conditions of a leg and to give additional support and prevent from shifting due

to scanner's vibrations.

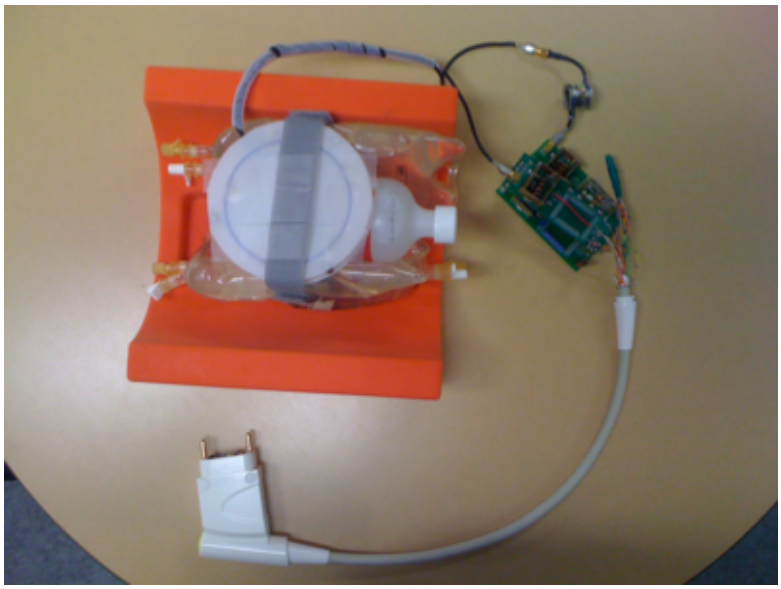

Figure 16 - **Phantom positioning, using only one phantom.**

When a human participant was recruited for data acquisitions, the coil was strapped under his calf, one inch below the knee junction. Between the two loops of the coil, was placed a vitamin pill to serve a reference on MR images. To maximize signal and avoid peak splitting, the coil is not placed directly over the separation between the two-gastrocnemius muscles. The following pictures gives an axial view of this positioning. The reference pill gives the position in proton localizer images of the center of the coil. This is used to align the FOV and coil's center to one another on proton images before phosphorus image acquisitions.

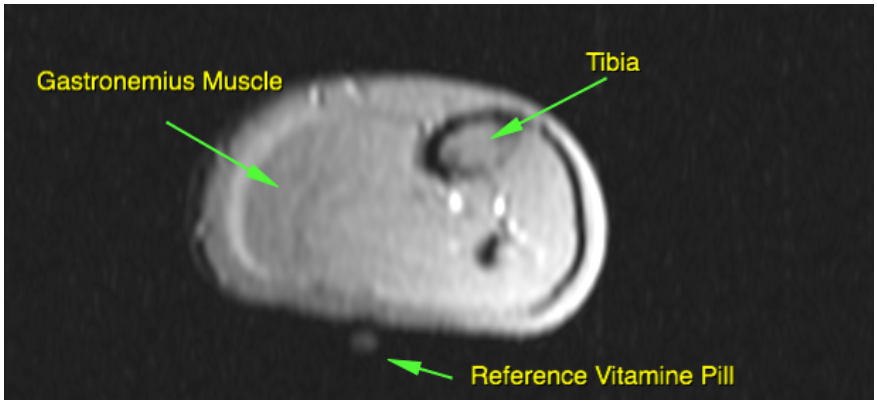

Figure 17 - Axial proton slice of a human calf muscle used for coil positioning.

Results acquired with smaller loop

Transmission voltage calibration

Data collected was processed using home made scripts in MATLAB. Individual spectrum was phased before being fitted with a Lorentzian curve. The area under curve was calculate for each increment of voltage, and plotted on the graph below.

The figures 18 and 19 give an example of curve fitting for both a phantom of high concentration (100mM) and a human calf.

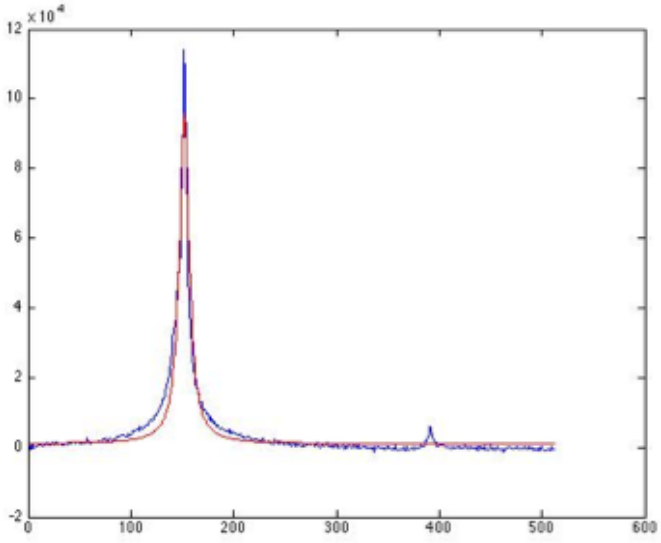

Figure 18 - Example of curve fitting for phantom data 100mM (intensity in AU vs signal shift in Hz, the largest peak represents PO_4)

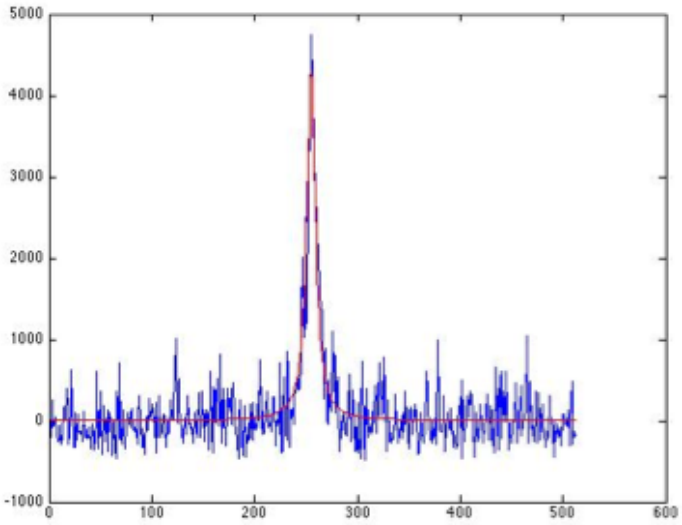

Figure 19 - Example of curve fitting on human data (intensity in AU vs signal shift in Hz, the largest peak represents PCr)

From the two previous images, it is possible to see that acquiring a spectrum on human model give much more noise signal than using a phantom. It is also worth mentioning that the reference between the two is different; PO4 for the phantom, and PCr for human.

The power curve obtained for the phantom with strongest signal and for a human subject is represented in figures 20 and 21. The intensity is in homogeneous arbitrary units, and voltages are represented by decade, in volts. For both the maximum signal was found to be 60Volts. This value was then set as default for phosphorus protocols with this coil. This value can be used as is for every test using this coil, or finer tuning of this value can be done before any acquisition. The optimal voltage is dependent on both subject and positioning, and recalibration could prove beneficial for spectroscopic acquisitions. Time being a huge constrain in MRI experiments, an automatic procedure to get optimal voltage for each subject could also be implemented as a new project.

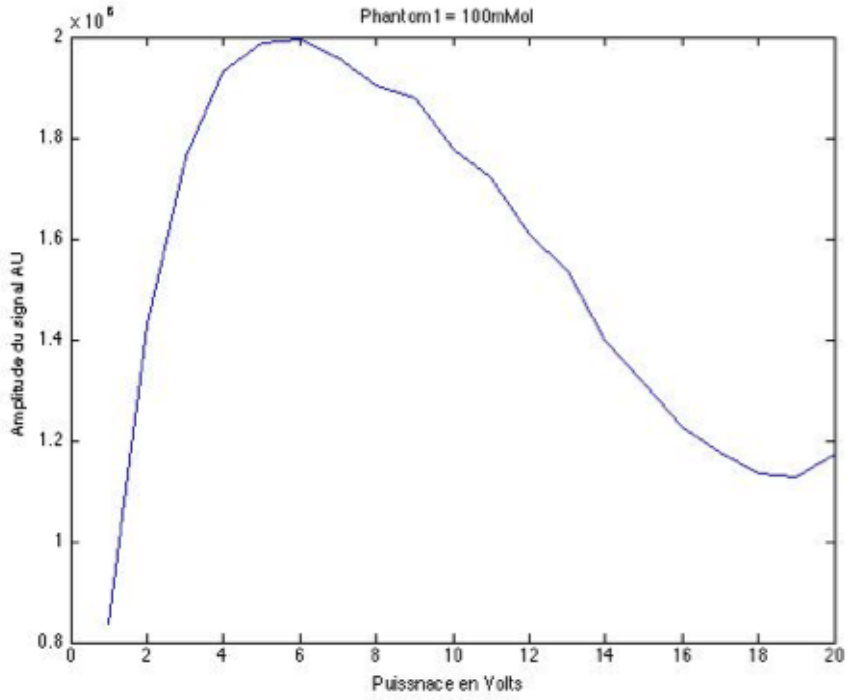

Figure 20 - Amplitude of the signal with increasing voltage using a 100mM phantom

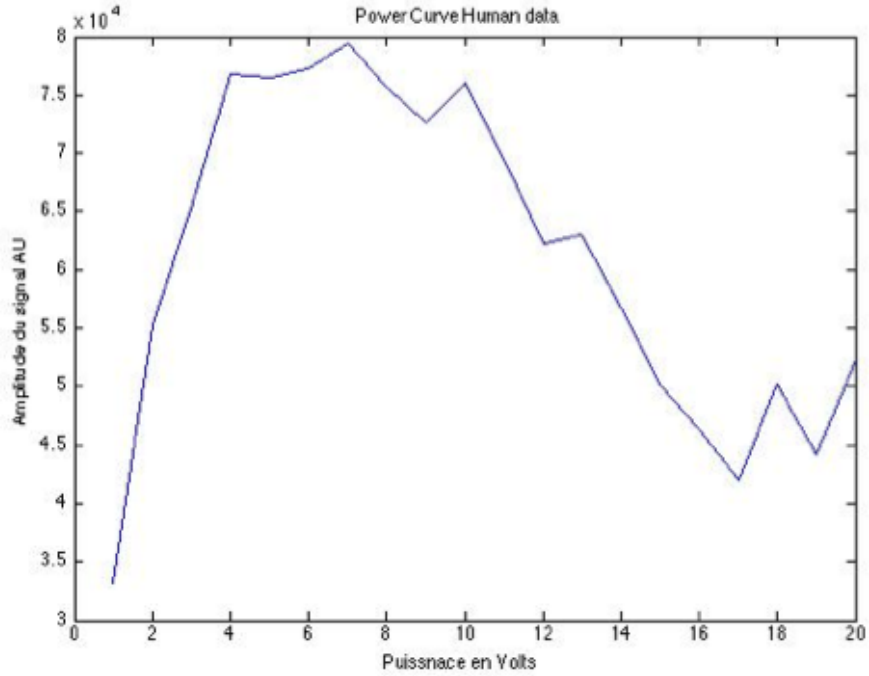

Figure 21 - Amplitude of the signal with increasing voltage with human subject.

B1 field and coil penetration

The next image is from the same phantom, one acquired using proton frequency with a volume coil, giving the full image over the field of view, and the overlay using the phosphorus frequency and the developed surface coil. The overlay image shows only a partial imaging of the phantom, the part that was sufficiently close to the coil to be excited during transmission. The next image shows that the phosphorus signal received comes from the 2.7cm closest to the coil. This is in accordance the rule of thumb stating that the penetration of a coil is the same than its radius. In our case, the radius of the coil is of 3cm. The visible indentation on the top of the bottle is due to air bubbles present in the phantom. To avoid this artifact, phantoms presenting residual air can be tilted so the air bubble is placed outside the field of view.

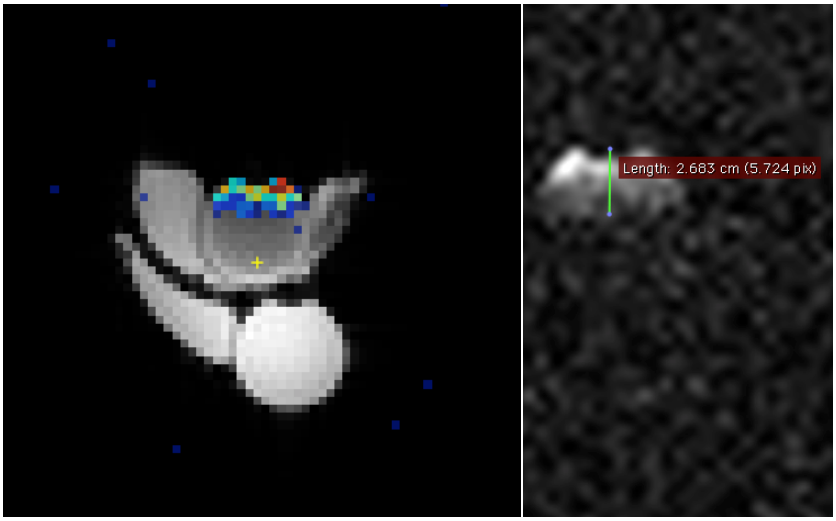

Figure 22 -- Overlay of phosphorus proton image (left) and phosphorus signal origin (right).

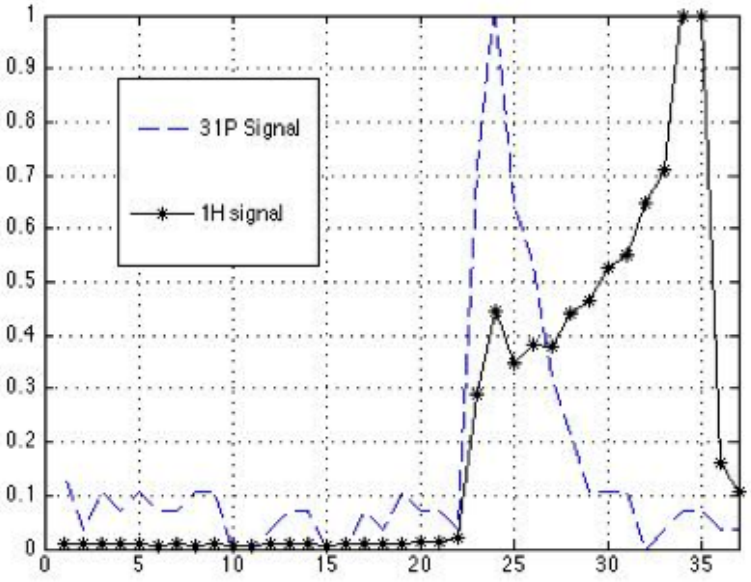

Figure 23 - Amplitude of the signal as a function of the position on an axial slice. The 31P coil is centered at 20 pixels.

Figure 23 gives the signal profile for both the proton volume coil and the phosphorus surface coil, from the top of the image to the bottom of the first bottle, along the middle axis, in pixels units. The signal was normalized dividing the pixel's value by the maximum value in each image. This representation helps see that only 6 pixels have signal larger than noise in the 31P profile. It also shows that signal is strongest in the middle of the field of view when using volume coil like it is the case with the 1H signal.

SNR on images

Figure 24 gives an example of the ROIs delimitation and the table below gives the SNR calculated for all three images.

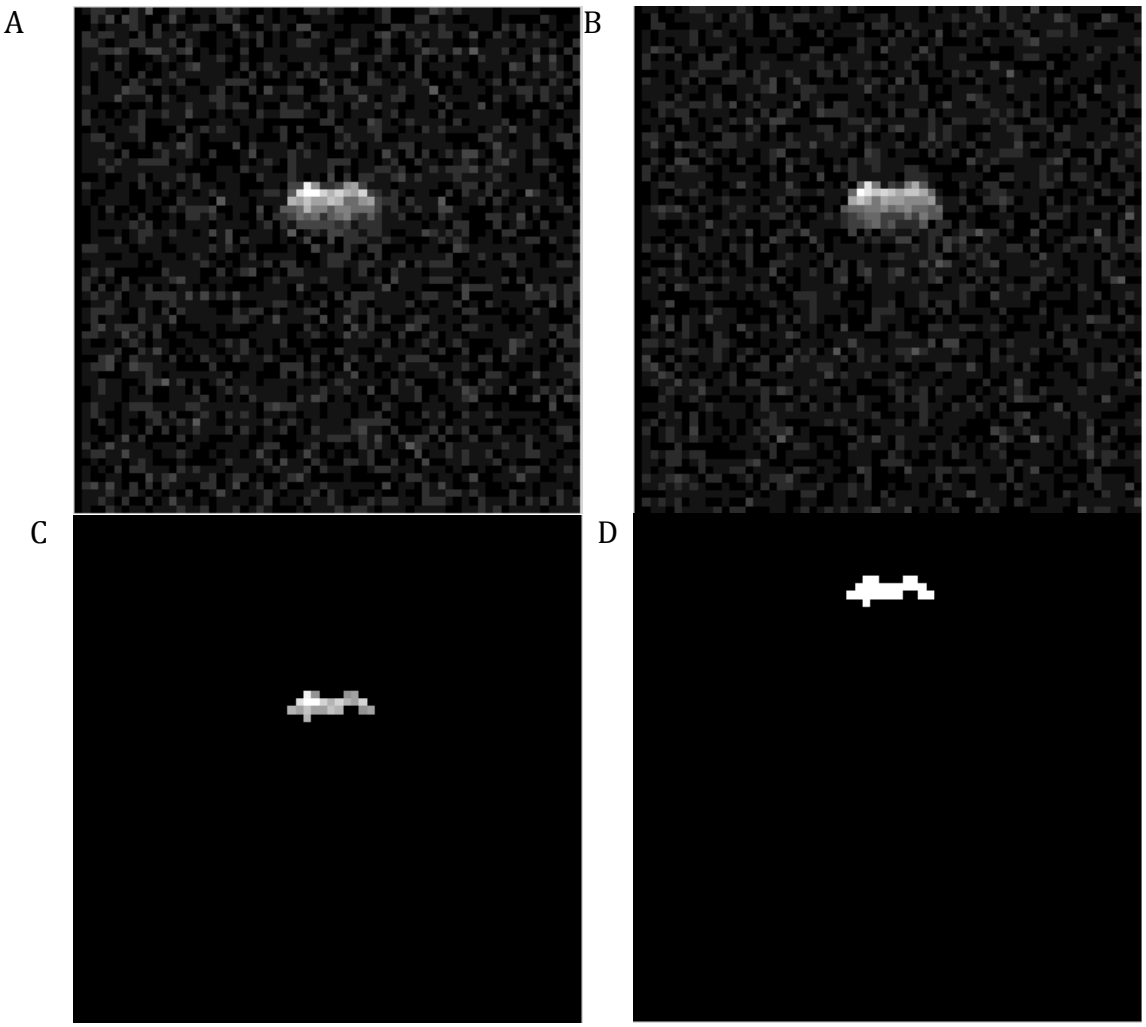

Figure 24 -31P FLASH images acquired consecutively (A, B), ROI of strongest signal (C) and ROI of of the same size over noise (D)

The second ROI in image D has the same area than the one is C. It was positioned to be exactly on the opposite side of the coil.

Table 2 – SNR for both acquisitions, and using the NEMA standard.

FLASH Images	SNR = (S-offset)/N
Acquisition 1	9.36
Acquisition 2	9.75
NEMA	6.598

The SNR is around 9.5, which is somewhat lower than expected values for surface coils. But the practical calculation of the SNR demands to use an ROI around 80% of the

phantom's surface to be significative. Since this is far form our case, we used the NEMA standard too. It gives a lower value, as expected, since it takes in account the differences in noise distribution. Nevertheless, the acquisition protocol was not adapted for ROI delineation, therefore, the calculated SNR which appears to be very low, should be recalculated using longer acquisitions with more averages, so that the full shape of the phantom can be approximated.

Larger single loop coil tuned to 31P

Geometry and general aspect

The design previously shown was made modular to allow replacement of the excitation and receiving loops only. A larger loop-set was designed to get deeper penetration into the studied object and to receive more signal.

Default transmission voltage

The calculations of the required transmission voltage give a good approximation of the voltages to get the optimal flip angles when using phosphorus sequence. Nevertheless, if it proves useful for preliminary calibrations, this voltage is subject dependent, and will need to be optimized for each acquisitions. An online optimization routine should be developed to assure exactitude of the used flip angle.

B1 field and coil penetration

As described previously, it is expected for the B1 field to penetrate the volume of interest by the same length than the coil's radius. With an exciting coil diameter of 10cm, the B1 field should excite atoms up to 5 cm in the volume. This should be enough for relevant studies of the calf and the visual cortex and other simple experiments. It allows the possibility of recruiting participants of various physiognomy, because with smaller penetration participants need to have very thin fat layers in between the coil and the object of interest (visual cortex, calf, …). On the other hand, this introduces a bias in the group populations to be studied.

SNR calculations

The SNR calculated gives a value that is fairly low compared to other surface coils in the literature. These calculations were based on a set of images that were acquired to prove feasibility of 31P MR acquisitions, and that were not appropriate to SNR calculations. It should be interesting to compare the coil's SNR to other coils once its design will be finalized and proper acquisition time will be dedicated to is characterization.

Discussion and future work

This working iteration of the coil's design gives promising results. Its capability to image the full scope of its expected penetration with relatively good enough signal makes it a great achievement in itself. It's testing on the scanner with phantom and human is a good exercise to demonstrate our new capability but also points certain limitations.

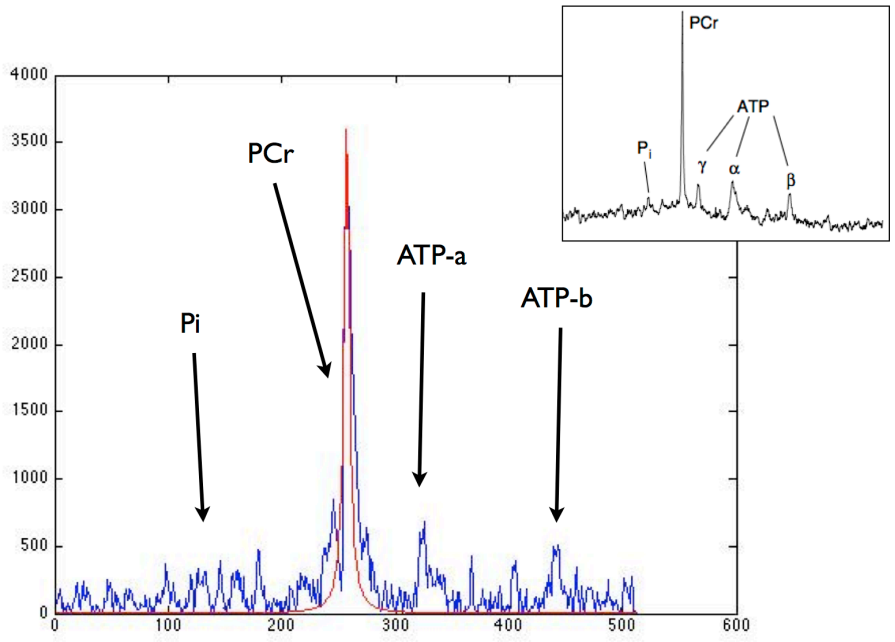

Figure 25 -Experimental results (in blue), with reference peak (in red) compared to reference spectrum from literature (in upper corner box)

The previous figure shows how closely our experimental results match literature references. This indicates that our current iteration would be sufficient to conduct meaningful studies but the fact that we have no direct way to optimize the transmission voltage is a problem that should be addressed before starting more oriented experiments.

Chapter 5: Phantoms

In addition to the measurement tools, test-objects had to be specifically designed to validate the sequences and the hardware we used. These test-objects are called phantoms and serve many purposes. On top of testing the hardware, they can be used to measure SAR limits (energy depositions) when developing sequences and avoid adverse heating in the human body. They finally can be used for calibration purposes, in MR spectroscopy, when signal only gives a relative quantification of metabolites. Phantoms of known concentration give the additional information to compare metabolites on an absolute scale.

Experimental design

Phantoms can take many sizes and form, but for practical and economical reasons we have decided to start with aqueous solutions enclosed in plastic bottles. The use of chemical preservatives like sodium-azide has been considered unnecessary for the preliminary tests.

For testing the equipment, a simple phosphorus solution was thought to be enough to get robust signal. It is relatively easy to create such a solution with a diluted phosphorus compound. We first started with a large plastic container of 1L of water in which was diluted granules of phosphate from over-the-counter fertilizer. In order to get the maximum signal, the solution was saturated and the phantom presented a deep blue coloring with white deposits at the bottom. Although this first phantom was large and fairly economic to create it failed to react as expected in an MR environment. This phantom will be referred to as Phantom-0.

Two additional phantoms were made. The two solutions were derived from existing recipes used in proton spectroscopy for making calibration basis-set (Provencher 2011). This recipe uses a buffer solution containing potassium phosphate salts in mono- and dibasic states. The dynamic equilibrium of the two, mixed with respective concentration of 28M and 78M assures a neutral pH of 6.8. This value was controlled using a pH-meter.

With the phosphate salts ratio kept constant, the first phantom was made to get a total concentration of PO4 of 100mM. For future reference, this high concentration bottle will be named Phantom-1. This high concentration was chosen because it is equal to a concentration of phosphorus ten times of what is found in the human body. It is used to validate the coil's ability to detect phosphorus compounds. Using simple dilution of this buffer-mix in water, the second phantoms was made to have a total concentration of PO4 of 10mM to approximate a phosphate concentration of the same order of magnitude than the one found in the human body. This phantom is used to validate the coil's ability to detect phosphorus compounds of the same concentration than in the human body. This second phantom was named Phantom-2.

Experimental results

The first phantom created, Phantom-0, was used with the *fid sequence and with manual adjustments fid sequences but failed to give enough signal for calibration and imaging purposes. When tested using regular proton sequences, it also failed to give any usable signal, having its strongest peak barely higher than noise level.

Various sequences and coils used where tested on the two other phantoms prior being used on human subjects. As expected, the signal received from Phantom-1 was greater by approximately ten times the signal received from Phantom-2.

Discussion

The concentration of Phantom-0 was in fact too high to get any picture or signal. One would think that the more phosphate there is in the phantom, the more signal the later gives. This is true in an environment in which the shielding effect is relatively low. In a saturated environment, the electrical bounds between phosphate and water molecules can be strong enough to create a magnetic shield for individual proton and phosphorus atoms. With fewer atoms reactive to changes in the magnetic field, their contribution to the magnetization vector is much smaller. This vector is reduced to its minimum and its changes are barely received by the coils. Phantom-0 was discarded and additional phantoms were made.

Signal received from Phantoms-1 and -2 was robust enough to continue testing with both of them. With its high concentration, Phantom-1 can test if the experimental set-up is sound and if it can detect any signal. With a lower concentration, Phantom-2 is a great tool to test if the set-up is sensitive enough to receive the signal of the same amplitude than expected with a human model.

Future Work

The two phantoms used here are robust enough to assess of the feasibility and the quality of the coil and the sequences being tested but they can only discriminate between "working" and "not working" state of a given experimental set-up. If one wants to effectively calibrate the given received signal in absolute units (mM), more precise and stable solution must be created. Additional on the phantoms should be gathered, like their T1, T2 constants. Additional phantoms should not be necessary for imaging applications. In order to calibrate the minimum spatial resolution of the coils, phantoms with inserts and specific geometries could be used, but phosphorus imaging is much noisier than proton imaging, and this task may prove highly time consuming for very few addition information.

In spectroscopic application, it is possible to compare metabolite concentration and ratios without needing of additional phantoms. However, a basis-set will be needed for absolute quantification. A basis-set is a set of phantoms where all expected metabolites in the image spectrum are diluted in a stable solution, in known concentration, in separate phantoms. A final phantom with all the metabolites can be added to the set to give additional information about possible interaction between metabolites. The signal of the measured metabolites can then be compared to the basis-set to get the absolute quantification. If this method is the most rigorous, it is also the most expensive since metabolites like ATP are cost prohibitive and hard to stabilize in solutions. To get the absolute quantification, computer modeling of the basis-set can be cheaper yet still acceptable procedure. Readily available software made for the scientific community, like Gamma, can be used.

The phantom development is the last development needed to test a coil before it is used to conduct meaningful MR spectroscopy experiments. The next chapter presents the next phase of the projects, and should give some ideas about what can be done with such a coil.

Chapter 6: Discussion - Future work

Overview of work

Coils development

The previous chapters have discussed the work done towards developing and testing of a new MR surface coil tuned to phosphorus resonance frequency. If some iteration on design and size has already been done, much work is still needed before a functional surface coil can be used for metabolism exploration. Nevertheless, the functional prototype may prove of good use for some preliminary explorations or phantoms and sequences development. In a near future the coil should be double-tuned to include decoupling capabilities. Another coil, a volume one, should also emerge from the completion of this project to give access to deeper anatomies like needed for brain imaging.

Phantom development

The set of phantoms developed in this project should be sufficient to continue testing of coils and sequences. The only additional phantoms that could be required would be calibration phantoms for a basis set. As explained in chapter 5, theses calibration phantoms can prove costly and are usually limited in their lifespan. Instead of making one phantom for each metabolite to be imaged, making one reference phantom of the strongest peak could prove an economic solution where all other absolute concentrations could be derived by ratio. Another solution could be to use simulated basis sets in order to save preparation and scanning costs. This solution is acceptable yet it is not as rigorous because it doesn't take in account the scanner's specificity, which can be a source of systematic error on the data.

Sequence development

During the project, some work has been done to find the optimal parameters to use prior acquiring data, like transmission voltage optimization. When using proton spectroscopy, these parameters can be optimized online using additional plug-ins on a

few sequences. These online optimizations help give robust spectra and should be transferred to phosphorus protocol. To be able to make theses online adjustments, some sequences programming could be a good investment.

Since the scanner is equipped with very few multi-nuclear sequences at the moment, developing expertise in sequence programming can also prove interesting if more complex protocols are to be tested, like multiple echo sequences, chemical shift imaging, or better localization and decoupling.

PCr recovery experiment

With a working coil, the first functional spectroscopy experiment to be done should be plantar extension. The monitoring of PCr depletion and regain once the work stops is a well documented physiological process that can help test coils, sequences and post-processing. In preparation of such an experiment, some work has been done with a group of students from École Polytechnique de Montréal.

Experimental set-up

This group of students in their final year in biomedical engineering had the mandate to build an isokinetic MR compatible pedal to be used for plantar extensions. After the one year they had to complete the project, they handed-in a wooden pedal connected to a pneumatic chamber in which the pressure rises as the participant execute plantar extensions. Their prototype is equipped with a data acquisition program that can be synchronized with the scanner, in order to register the force applied to the pedal in time.

The coil is to be placed under the calf muscle, one inch lower than the knee, where the muscle is the biggest.

The pedal is mounted on a wooden board fixed to the table via the holes running along its sides. To minimize movement, the legs strapped by Velcro's elastics and placed in a way to avoid overlapping in the image due to wrap-around effect during encoding.

The participants should be asked to execute plantar extensions over a period of 1 to 2

minutes, until exhaustions, and repeat after the same amount of time for rest. Using up to 4 subjects over an exercise period of 30 minutes, there should be enough signal to clearly observe the phenomenon. Additional rapid low resolution images, like single shot EPI, can be added in between spectroscopy segments to monitor for major movement that would help discard certain spectrum.

Sequence: fid

The sequence to be used in this experiment is a non-localized fid. This sequence should give maximum signal and give access to very short TE. This sequence is already available and tested on the scanner.

Expected results

It is expected to observe the depletion of phosphocreatine during the exercise and it's replenishing as soon as this exercises stops. The same experiment can be used to compare optimal parameters, protocol flow, decoupling effects, and so on. Because the underlying observed physiology is highly dependent on blood flow, this experiment can be used to test the protocol's time sampling and parameters against the physiological respond before trying the same experiment in the brain where such questions can be harder to ask. This type of experiment can be used to observe phosphorus exchanges between phosphorus metabolites in the brain under activation. ATP consumption and generation can be monitor to asses ischemia or mitochondrial dysfunctions.

Conclusion

Human energy metabolism has been studied extensively in muscles, but additional research is needed to understand its organization in the brain. The challenge becomes even more pressing when age-related mitochondrial dysfunctions are being associated with diseases like Alzheimer's and Parkinson's that have increasing incidence in the population. To address such questions it is imperative to develop MRI tools capable of probing the energy metabolism.

Magnetic resonance offers the possibility to image and monitor metabolism non-invasively, and can be part of the new diagnostics solutions. Because proton magnetic resonance is blind to the key molecules of the human metabolism, there is a need to develop adapted tools to help researcher in their endeavor.

We have designed a first prototype of a phosphorus-tuned magnetic resonance coil. For testing purposes we also make two phantoms that can be used as crude imaging reference. The coil has a small surface area and is able to image anatomies in its close neighborhood. It can be used to conduct meaningful spectroscopy experiments using unlocalized sequences.

This first step should be followed by the new design of a larger surface coil, implementation of double tuning capabilities and testing of additional sequences that allow for localization spectroscopy. Given the necessary support, this project can be the first step along great discoveries in the phosphorus metabolism both in healthy and diseased models.

Bibliographie

Bélanger, M, I Allaman, and P J Magistretti. 2011. “ScienceDirect.com - Cell Metabolism - Brain Energy Metabolism: Focus on Astrocyte-Neuron Metabolic Cooperation.” *Cell metabolism*.

Clark, J B. 1998. “*N*-Acetyl Aspartate: a Marker for Neuronal Loss or Mitochondrial Dysfunction.” *Developmental Neuroscience* 20(4-5): 271–76.

De Graaf, Robin A. 2008. *In Vivo Nmr Spectroscopy*. Wiley-Interscience.

Fox, P T, and M E Raichle. 1986. “Focal Physiological Uncoupling of Cerebral Blood Flow and Oxidative Metabolism During Somatosensory Stimulation in Human Subjects..” *Proceedings of the National Academy of Sciences of the United States of America* 83(4): 1140–44.

Gu, M, J M Cooper, J W Taanman, and A H Schapira. 1998. “Mitochondrial DNA Transmission of the Mitochondrial Defect in Parkinson's Disease..” *Annals of neurology* 44(2): 177–86.

Hoa, Denis. 2007. *L'irm Pas a Pas*.

Hu, Simon, Asha Balakrishnan, Robert A Bok, Brittany Anderton, Peder E Z Larson, Sarah J Nelson, John Kurhanewicz, Daniel B Vigneron, and Andrei Goga. 2011. “13C-Pyruvate Imaging Reveals Alterations in Glycolysis That Precede C-Myc-Induced Tumor Formation and Regression..” *Cell metabolism* 14(1): 131–42.

Jack, Clifford R, David S Knopman, William J Jagust, Leslie M Shaw, Paul S Aisen, Michael W Weiner, Ronald C Petersen, and John Q Trojanowski. 2010. “Hypothetical Model of Dynamic Biomarkers of the Alzheimer's Pathological Cascade..” *Lancet neurology* 9(1): 119–28.

Lange, T, U Dydak, T P L Roberts, H A Rowley, M Bjeljac, and P Boesiger. 2006. “Pitfalls in Lactate Measurements at 3T.” *American journal ...*.

Magistretti, Pierre J, and Luc Pellerin. 1999. “Astrocytes Couple Synaptic Activity to Glucose Utilization in the Brain.” *Physiology*.

Mangia, Silvia, Ivan Tká, Nikos K Logothetis, Rolf Gruetter, Pierre-Francois Van de Moortele, and Kâmil Uğurbil. 2007. “Dynamics of Lactate Concentration and Blood Oxygen Level-

Dependent Effect in the Human Visual Cortex During Repeated Identical Stimuli." *Journal of Neuroscience Research*.

Mangia, Silvia, Ivan Tkác, Rolf Gruetter, Pierre-Francois Van de Moortele, Bruno Maraviglia, and Kâmil Uğurbil. 2007. "Sustained Neuronal Activation Raises Oxidative Metabolism to a New Steady-State Level: Evidence From 1H NMR Spectroscopy in the Human Visual Cortex.." *Journal of cerebral blood flow and metabolism : official journal of the International Society of Cerebral Blood Flow and Metabolism* 27(5): 1055–63.

Martin, W R Wayne. 2007. "MR Spectroscopy in Neurodegenerative Disease.." *Molecular imaging and biology : MIB : the official publication of the Academy of Molecular Imaging* 9(4): 196–203.

Mosconi, Lisa, Valentina Berti, Lidia Glodzik, Alberto Pupi, Susan De Santi, and Mony J de Leon. 2010. "Pre-Clinical Detection of Alzheimer's Disease Using FDG-PET, with or Without Amyloid Imaging.." *Journal of Alzheimer's disease : JAD* 20(3): 843–54.

NEMA, M S. 2008. "NEMA: Determination of Signal—to—Noise Ratio... - Google Scholar." *NEMA Standard Publication MS*.

Pellerin, Luc, Giovanni Pellegri, Philippe G Bittar, Yves Charnay, Constantin Bouras, Jean-Luc Martin, Nephi Stella, and Pierre J Magistretti. 1998. "Evidence Supporting the Existence of an Activity-Dependent Astrocyte-Neuron Lactate Shuttle." *Developmental Neuroscience* 20(4-5): 291–99.

Piaceri, Irene, Valentina Rinnoci, Silvia Bagnoli, Ylenia Failli, and Sandro Sorbi. 2012. "Mitochondria and Alzheimer's Disease.." *Journal of the neurological sciences* 322(1-2): 31–34.

Provencher, S W. 2011. "LCModel & LCMgui User's Manual." *LCModel Version*.

Stork, C, and P F Renshaw. 2005. "Mitochondrial Dysfunction in Bipolar Disorder: Evidence From Magnetic Resonance Spectroscopy Research." *Molecular psychiatry* 10(10): 900–919.

Vander Luciano, Sherman, and Stuart Ira Fox. 1992. *Human Physiology*. WCB/McGraw-Hill.

Wallace, D C. 2012. "Bioenergetic Origins of Complexity and Disease." *Cold Spring Harbor Symposia on Quantitative Biology* 76(0): 1–16.

Wallace, Douglas C. 2005. "A Mitochondrial Paradigm of Metabolic and Degenerative Diseases, Aging, and Cancer: a Dawn for Evolutionary Medicine.." *Annual review of genetics* 39: 359–407.

Westerblad, Håkan, David G Allen, and Jan Lännergren. 2002. “Muscle Fatigue: Lactic Acid or Inorganic Phosphate the Major Cause?.” *News in physiological sciences : an international journal of physiology produced jointly by the International Union of Physiological Sciences and the American Physiological Society* 17: 17–21.

Wijnen, J P, T W J Scheenen, D W J Klomp, and A Heerschap. 2010. “31P Magnetic Resonance Spectroscopic Imaging with Polarisation Transfer of Phosphomono- and Diesters at 3 T in the Human Brain: Relation with Age and Spatial Differences..” *NMR in biomedicine* 23(8): 968–76.